Surface Dynamics of the Intermetallic Catalyst Pd_2Ga, Part I – Structural Stability in UHV and Different Gas Atmospheres

Gregor Wowsnick[1], Detre Teschner[1], Igor Kasatkin[1], Frank Girgsdies[1], Marc Armbrüster[2], Aiping Zhang[2], Yuri Grin[2], Robert Schlögl[1], Malte Behrens[1*]

[1] Department of Inorganic Chemistry, Fritz-Haber-Institut der Max-Planck-Gesellschaft, Faradayweg 4-6, 14195 Berlin, Germany

[2] Max-Planck-Institut für Chemische Physik fester Stoffe, Nöthnitzer Str. 40, 01187 Dresden, Germany

**Corresponding author:*

Malte Behrens, Department of Inorganic Chemistry, Fritz-Haber-Institut der Max-Planck-Gesellschaft, Faradayweg 4-6, 14195 Berlin, Germany, behrens@fhi-berlin.mpg.de, phone: +493084134408

Abstract

The structural and electronic properties of unsupported Pd_2Ga were investigated after different pre-treatments. Pd_2Ga provides with respect to elemental Pd a significantly modified electronic structure with its d-band centre being shifted away from the Fermi level. It was found that the electronic structure of the surface depends strongly on its pre-treatment and on the chemical environment. We report a detailed bulk and surface characterization of the intermetallic compound by means of XRD, DTA/TG/MS, SEM, XPS and HR-TEM. At moderate temperatures the bulk of Pd_2Ga is chemically resistant against H_2 or O_2 atmosphere and against mechanical load. Contrariwise its surface is highly sensitive against even traces of oxidizing agents leading quickly to a disparity between bulk and surface structure and composition. The reversibility of this dynamic effect depends on the degree of decomposition and on the sample history. An almost pure intermetallic surface can only be achieved in highly reducing atmospheres.

Keywords: selective hydrogenation, Pd, Pd_2Ga, intermetallic compounds, electronic structure, d-band shift, near ambient pressure XPS, in situ stability, surface dynamics

1. Introduction

The selective hydrogenation of alkynes to alkenes are applied in hydro-refining processes to remove impurities of acetylene or methylacetylene in corresponding alkene streams[1], or in industrial fine chemical syntheses, e.g. of Linalool, Vitamin A, E and K or insect pheromons[2,3,4].

Pd based catalysts provide an outstanding activity and selectivity for the hydrogenation of alkynes[5,6,7,8]. However, they can act in selective as well as an unselective manner (for further

discussion see SI). In general, there are three main influences discussed, which determine the desired selectivity of Pd towards the alkene. Firstly, there is a geometric effect[9]: The isolation of active sites and the presence of exclusively small ensembles of active atoms leads to the suppression of reactions requiring larger ensembles, e.g. oligomerization or formation of strongly bound hydrogen deficient species[10], in general known as ensemble effect[11,12]. In particular the presence of only small ensembles reduces the availability of hydrogen[13] and hinders over-hydrogenation. Secondly, Pd easily forms Pd hydrides[14]: Compared to dissociatively bonded H atoms on the surface, the hydrogen incorporated in the subsurface or in the bulk of Pd provides a higher reactivity and lowers the selectivity towards the alkene due to enhanced alkene hydrogenation[15,16,17,18]. Thirdly, the selectivity could be increased if an electronic effect enhances the barrier for alkene hydrogenation and thus favoring alkene desorption[19].

Recently, it has been shown that the selective phase in an initially pure Pd catalyst during hydrogenation of C-C triple-bonds is not the pure Pd itself but an *in situ* formed subsurface palladium-carbon phase formed by a rapid decomposition of the substrate as a first step of the reaction[20,21]. The subsurface C modifies the electronic structure of Pd at the surface and slows down diffusion of H through the Pd-C surface phase into the Pd lattice. It weakens the adsorption strength of surface bonded H and thus further lowers the availability of H at the surface. As a result, over-hydrogenation and formation of the alkane is suppressed on this modified surface. Unfortunately, the existence of the Pd-C phase is highly dynamic and depends strongly on the chemical potential of C and H[18]. High potentials of H or low potentials of the acetylene lead to hydrogenation of the subsurface C and, hence, Pd loses its selectivity.

Thus, less volatile additional modifiers are frequently added. In the semi-hydrogenation of acetylene eggshell Pd-Ag/Al_2O_3 alloy catalysts are applied[22,23], while Lindlar's catalyst[24],

optionally poisoned with organic nitrogen bases, is one of the most common catalysts in liquid phase hydrogenation reactions. Beside the insights in the reaction mechanisms of acetylene hydrogenation over Pd under typical low pressure conditions, the role of different modifiers and additives, is still controversially discussed and they are, as described briefly by means of Pd-Ag alloys and CO in the SI, not necessarily stable under reaction conditions. This is likewise the case for Pd catalysts in liquid phase hydrogenations of alkynes. Although, it is not always sufficiently stable and selective[25], for instance, if H_2O is used as solvent. Furthermore, impregnated heavy metals can be subjected to a dynamic redox chemistry and can leach and C-N bonds of organic bases could be cleaved by hydrogenolysis in presence of Pd[26]. Works of Mallat et al.[27] and López et al.[28] highlight the role of important modifiers. It is still necessary and a challenge to find catalyst materials, which are not reliant on a complex subsurface chemistry or additional modifiers. Recently, CeO_2 was found to be highly active in the gas phase hydrogenation of methylacetylene[29] without the use of typical hydrogenation active transition metals.

Intermetallic compounds (IMCs) like Pd_3Pb[30] or NiZn[19] were discussed as alternative catalyst for acetylene hydrogenation with their well-ordered crystal structure and their modified electronic structure. The modification of the electronic structure of Pd and Ni IMCs is generally stronger compared to substitutional alloys[11,31] or for non-stoichiometric surface phases. This effect is more pronounced with decreasing electronegativity of the second metal[32,33]. In the last years Pd-Ga intermetallic compounds were found to be stable and selective catalysts for the semi-hydrogenation of acetylene[34,35,36]. It was shown, that the ordered structure and the partially covalent bonds of these intermetallic compounds gives rise to the intrinsically modified electronic structure compared to elemental Pd. Detailed studies have been carried out for PdGa where covalent interactions between Pd and Ga lead to a shift of the Pd 4d band centre away from the Fermi level, which has been confirmed by XPS and

NMR studies[37,38]. An increasing d-band shift away from the Fermi level with increasing gallium content was proven for Pd_2Ga, PdGa and Pd_3Ga_7 by XP spectroscopy in the valence band region[40]. The partially covalent chemical bonding in these materials leads to an enhanced structural stability suppressing a dynamic subsurface chemistry. PdGa exhibits an ordered crystal structure where Pd atoms are fully surrounded by Ga atoms resulting in expanded Pd-Pd distances compared to elemental Pd[39]. Various bulk and surface sensitive methods, applied *ex situ* and under reaction conditions, like XRD, EXAFS, DTA and XPS supported the stability of PdGa and Pd_3Ga_7 and emphasized the similarity between bulk and surface[34,35,36]. Theoretical calculations supported the superior catalytic properties of PdGa systems[19].

A significant d-band shift is also observed for Pd_2Ga[40] but, different from PdGa, Pd_2Ga does not show a perfect site-isolation. Pd_2Ga crystallizes in the Co_2Si-type structure (space group *Pnma No. 62*, orthorhombic, see Figure 1)[41]. The two symmetrically nonequivalent positions of Pd are both surrounded by eight Pd atoms with distances of 2.82-2.99 Å, which is slightly enlarged compared to elemental Pd (2.75 Å)[42]. Five Ga atoms with Pd-Ga distances between 2.54 and 2.84 Å complete the first coordination sphere. Thus, there is only a partial isolation of Pd by Ga in the first coordination sphere and triangular arrangements of Pd – similar to elemental palladium – are still present. In contrast to PdGa and Pd_3Ga_7, Pd_2Ga exhibits a significant homogeneity range ($Pd_{2+x}Ga_{1-x}$, $-0.04 \leq x \leq 0.02$ at 500 °C). In the Pd richer regime Pd atoms partially substitute Ga positions. Wannek et al.[43] draw up the structural relationship between the Co_2Si-type like $Pd_{2+x}Ga_{1-x}$ and a fcc solid solution Pd_xGa_{1-x}. However, a metallurgically prepared powdered Pd_2Ga sample without pre-treatment also shows a high selectivity in the hydrogenation of acetylene and provides the same long-term stability[44] as in the case of PdGa and Pd_3Ga_7. In contrast to the more Ga-rich materials, one advantage of Pd_2Ga is that it can be obtained comparably easy way in a highly active

nanostructured form by co-reduction of Ga oxide supported Pd. For instance, a $Pd_2Ga/MgO/MgGa_2O_4$ catalyst was shown to maintain the higher selectivity compared to monometallic Pd nanoparticles[45]. However, in the latter case, an unusual activation period of this catalyst over 40 hours has been observed before stable performance was reached. Such dynamic behavior might be related to an *in situ* change of the material surface. Haghofer et al.[46] found a poor long-term stability of supported nanoparticulate Pd_2Ga in methanol steam-reforming due to decomposition of the intermetallic surface under these conditions. In a combined *in situ* XRD, *in situ* XAS and CO-FTIR study[47] under H_2 and O_2 atmosphere, the *in situ* formation of hydrides could be excluded but it was shown that the surface undergoes oxidative decomposition in O_2 forming Ga oxides and elemental Pd or a Ga depleted Pd_2Ga phase. Evidence for the structural disturbance of the surface due to oxidative decomposition was also reported in a HR-TEM study of unsupported Pd_2Ga nanoparticles[48]. The close structural relationship between the compounds makes a straightforward distinction by HR-TEM challenging. However, larger accumulations of elemental Pd were not observed on the surface but an ordered and potentially fcc structured, only slightly Pd-enriched Pd_2Ga phase was suggested. These observations induce doubts with respect to the pronounced stability also of the unsupported, bulk Pd-Ga intermetallic compounds. The first experiments to determine the catalytic properties of powdered, unsupported Pd_2Ga and PdGa in the liquid phase hydrogenation of phenylacetylene, which were partly already reported in [49], did not show significant differences in selectivity towards styrene compared to elemental Pd powder (see part II of this work[50]). This observation further suggests that the modified catalytic properties of the intermetallic compounds PdGa and Pd_2Ga, whose surfaces were reported to be unchanged before and during the gas phase hydrogenation of acetylene at high temperatures (T = 200 °C), are not present under the conditions of liquid phase hydrogenation

at room temperature and provoked us to study in detail the stability of pure, metallurgically prepared Pd_2Ga in different chemical environments.

Here we address the question, whether Pd_2Ga with its strong intrinsic modification of the d-band can transform its properties into chemical reactivity. In part I of this work, several bulk- and surface sensitive methods were applied with special focus on the resistance against oxidation, participation of sub-surface chemistry and its mechanical stability. Therefore, metallurgically prepared bulk-samples of Pd_2Ga in absence of supports or modifiers have been applied as model catalysts. This allowed studying the stability of the intermetallic compound and the potential of its intrinsically modified (electronic) structure for application. Part II[50] focuses on the correlation of the surface structure with the catalytic properties in the selective hydrogenation of phenylacetylene in the liquid phase.

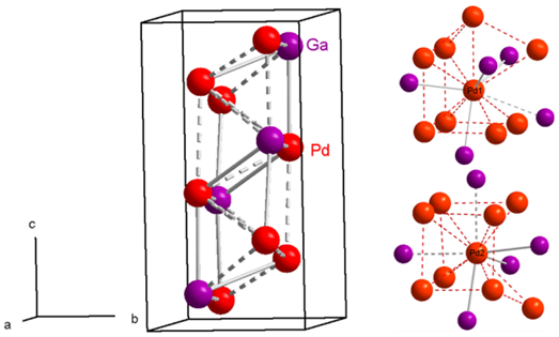

Figure 1: Left: Unit cell of Pd_2Ga. Top right: First coordination shell of Pd1. Down right: First coordination shell of Pd2. The compound crystallizes in the Co_2Si type of structure. The short Pd-Ga distances (2.54-2.62 Å) are shown as full lines, dashes lines represent atomic distances between 2.81-2.99 Å. Structural motifs of elemental palladium, i.e. Pd-triangles, are preserved within the crystal structure.

2. Materials and Methods

2.1 Synthesis of Pd_2Ga

Pd_2Ga was synthesized by melting stoichiometric amounts of Pd granules (Chempur, 99.95%) and Ga pellets (Chempur, 99.99%) in a glassy carbon crucible in a high frequency induction furnace under Ar atmosphere in a glove box (O_2 < 1 ppm, H_2O < 1 ppm). The obtained regulus was annealed at 800 °C in an evacuated quartz glass ampoule for three days.

A metallographic specimen was prepared by cutting 1 mm thick cylinders from the regulus. The slice was polished and stored under Ar. To obtain a fine powder of Pd_2Ga the material was either ground in air in an agate mortar or the material was powdered in air in a swing mill (*Retzsch*, MM 200, 4 ml WC pot with two WC balls, 25 Hz) two times for 30 min with a break of 20 min. The absence of any additional phases was verified by X-ray powder diffraction and, in the case of the metallographic specimen, by optical microscopy and scanning electron microscopy.

2.2 X-ray powder diffraction

For *ex situ* X-ray powder diffraction the sample was placed on a 3 μm Kapton foil covered with vaseline. The measurement was performed on an image plate Guinier camera (G670, Huber, Cu $K\alpha_1$ radiation, λ = 1.54056 Å, curved Ge monochromator, $3° < 2\Theta < 100°$, CCD detector). For determination of lattice parameters the powder was mixed with LaB_6 as internal standard (a = 4.15695(6) Å) prior to spreading on the Kapton foil. *In situ* X-ray powder diffraction was performed on a on a STOE theta/theta X-ray diffractometer ($CuK\alpha_{1+2}$ radiation, secondary graphite monochromator, scintillation counter) equipped with an Anton Paar XRK 900 *in situ* reactor chamber. The gas feed was mixed by means of Bronkhorst mass flow controllers, using helium as inert balance gas at a total flow rate of 100 ml/min. The effluent gas composition was monitored with a *Pfeiffer* OmniStar quadrupole mass spectrometer.

XRD data were evaluated by total pattern analysis using the TOPAS software[51]. The fitting procedure was based on the Rietveld method[52] using the Pd_2Ga crystal structure model of Kovnir et al.[41].

2.3 Metallography and scanning electron microscopy

For metallographic analysis samples were embedded in a conductive polymer (Polyfast®, Struers), abraded with SiC paper and subsequently polished with diamond paste (minimum size 0.25 μm). The single phase nature of the material was confirmed by light microscopy (Axioplan 2, Zeiss) and scanning electron microscopy (Cameca microprobe SX100). WDX analysis was performed using a PdGa standard with known chemical composition (determined by ICP-OES) as reference. The particle morphology and homogeneity of the powdered samples was investigated by scanning electron microscopy using a Hitachi S4800 equipped with an EDAX Genesis 4000 detector.

2.4 Surface area characterization

The specific surface area was determined using Kr physisorption at 77 K in a Quantachrome AsiQ set-up by multi-point BET. Prior to the measurements samples where pre-treated either for 19 h in vacuum at ambient temperature or for 5 h at 400 °C in 5% H_2/Ar.

2.5 Transmission electron microscopy

A Philips CM200FEG microscope operated at 200 kV and equipped with a field emission gun, Gatan imaging filter, and energy-dispersive X-ray (EDX) analyzer was used. The coefficient of spherical aberration was Cs = 1.35 mm, and the information limit was better than 0.18 nm. High-resolution images with a pixel size of 0.016 nm were taken at the magnification of 1.083.000 × with a CCD camera, and selected areas were processed to obtain the power spectra (square of the Fourier transform of the image), which were used for phase identification by measuring interplanar distances (+/- 0.5 %) and angles (+/- 0.5 deg).

2.6 In situ thermal analysis

In situ DTA/TG/MS measurements were performed with a Netzsch STA 449 Jupiter system connected to a Pfeiffer Omnistar 300 mass spectrometer. 248 mg of milled Pd_2Ga were weighted under air and placed inside a corundum crucible. The temperature program is described in the results and discussion section. The total gas flow during the measurement was either 40 ml/min He or a mixture of 5 ml/min H_2 in 45 ml/min He.

2.7 X-ray photoelectron spectroscopy

Near ambient pressure X-ray photoelectron spectroscopy[53] was performed at the ISISS beamline at Bessy II, Helmholtz Zentrum Berlin. The metallographic specimen was prepared under Ar and transferred to the XPS chamber in a transport chamber without air contact. Approximately 250 mg of powdered samples were prepared by pressing the powder in air to a pellet with a diameter of 8 mm and a thickness of about 1 mm. Pellets of as prepared milled samples were introduced with air contact to the XPS chamber, while pellets of pre-reduced powder were annealed and reduced again for 1 h at 400 °C in 5% H_2/Ar and were subsequently transferred under Ar to the chamber. XPS measurements were performed under UHV (10^{-7} mbar) at temperatures between 25 °C and 400 °C or *in situ* in different atmospheres (H_2: Westfalengas, 99.999%; O_2: Westfalengas, 99.999%;) with a maximum total pressure of 1 mbar. Ga 3d, Pd 3d and C 1s core levels as well as the valence band region were recorded. Spectra were taken with various excitation energies corresponding to kinetic electron energies of 145 eV, 385 eV or 785 eV. Using 3-times the inelastic mean free path given for elemental Pd[54], these kinetic energies refer to an information depth of 1.3, 2.0 and 3.4 nm as a rough estimation. Analysis of the spectra was performed by the software CASA XPS[55]. For details concerning the peak-fitting see supporting information. Quantification was performed using energy dependent cross sections from Yeh and Lindau[56]. The peak intensities are normalized to the incoming photon flux.

3. Results and Discussion

In the present study three different kinds of Pd_2Ga samples were investigated: 1) A metallographic specimen, cut from compact regulus, 2) milled powder and 3) ground powder. The surface of the metallographic specimen was polished before analysis and handled exclusively under Ar atmosphere in a glove box. The ground and the milled Pd_2Ga samples were investigated in the as prepared state. Milled Pd_2Ga was subsequently subjected to different pre-treatments.

3.1 Characterization and stability of the bulk of Pd_2Ga

Single-phase Pd_2Ga was successfully prepared from the elements, as proven by XRD analysis of the ground sample (Figure 2). Metallographic analysis of the cross section of the regulus further verifies the absence of any additional minority phases (see Figure SI 1). Inhomogeneities were not detected for the polycrystalline metallographic specimen in the SEM analysis. The composition of the specimen according to WDX is $Pd_{66.2(\pm0.4)}Ga_{33.8(\pm0.1)}$. The lattice parameters of the ground Pd_2Ga are a = 5.4809(2), b = 4.0556 (1) and c = 7.7895(1) Å, which is in good agreement with reported literature data[41]. To decrease the particles size and increase the specific surface area, the material was milled in a swing mill. As shown in Table 1 and Figure 2 d, the milled powder provides, compared to the ground powder, significantly broader reflections. This is likely caused by the stress due to the harsh mechanical load during milling as already reported earlier in the case of PdGa[35]. The milled powder still remains single-phase, which was also confirmed by a Rietveld refinement (not shown) and the lattice parameters show only marginal changes (Table 1). According to SEM images (Figure SI 2) the particle size is in the range of 0.5-40 µm, and smaller particles cover

larger ones due to agglomeration. As determined by Kr physisorption, the specific surface area of the powder is 0.27±0.01 m^2g^{-1}. Elemental mapping in the SEM microscope reveals a homogeneous distribution of Pd and Ga (Figure SI 2 b). The average composition of the powder according to EDX is $Pd_{68(\pm3)}Ga_{32(\pm3)}$ in reasonable agreement with the WDX results obtained on the regulus. Small particles of tungsten carbide were also detected in very low quantity originating from abrasion during milling. After 4 h of temperature treatment at 400 °C in reducing atmosphere (5% H_2/Ar, 100 ml/min) the XRD reflections become sharp again reaching similar full width at half maximum (FWHM) values as by crushing the sample (Figure 2 d). This is expected since the melting point of Pd_2Ga is about 1200 °C and 400 °C lies above the *Hüttig* temperature where structural healing becomes a fast process[57]. SEM images (Figure S1 2 c) reveal a somewhat lower amount of small particles, but no dramatic changes in particle size and morphology. Also the specific surface area remains unchanged (0.28±0.01 m^2g^{-1}). Kohlmann[58] studied the structural stability of Pd_2Ga against hydrogen by *ex situ* XRD and *in situ* DTA under harsh conditions (p_{H2} = 375 bar, T = 250 °C, t = 60 h) and found no hints for the formation of hydrides. Also Haghofer et al.[47] found no hint for the formation of hydrides by *in situ* EXAFS experiments for a Pd_2Ga/Ga_2O_3 catalyst at room temperature. Because the stability of hydrides is strongly dependent on the temperature, we studied the *in situ* stability of the milled Pd_2Ga in H_2 atmosphere by DTA/TG/MS (Figure 3) under elevated, but comparably mild conditions. After desorption of surface-adsorbed H_2O at 200 °C in pure He atmosphere, during the second heating cycle in 10% H_2/He (total pressure 1 bar) an exothermic peak with an onset temperature at 180 °C is observed, which is accompanied by a mass loss of 310 µg and H_2O formation. We assign the water formation to the reduction of surface Ga oxide which is reduced to metallic Ga corresponding to ~1% of the total Ga content. Further signals could not be detected under these conditions when heating to temperatures up to 500 °C and cooling under He atmosphere again. Also a

subsequent long-time treatment in 10% H_2/He with stepwise increased temperature from 50 °C to 150 °C, i.e. in a temperature range where hydride formation and decomposition on elemental Pd takes place, revealed no significant thermal effects due to phase transformations. The bulk stability was furthermore investigated by *in situ* XRD in 100% He, 25% H_2/He and 20% O_2/He (details see Figure SI 3 and 4). No hints for phase transformations of the bulk in He and H_2 were observed during stepwise heating to 400 °C and subsequent cooling in agreement with the DTA/TG/MS measurement. Decomposition of the bulk starts at approximately 300 °C when treated in 20% O_2/He resulting in a mixture of Pd_2Ga, Pd_5Ga_3, Pd and PdO. Formed Ga oxide is probably amorphous and not detectable by XRD.

In summary, the bulk of Pd_2Ga provides a high mechanical as well as chemical stability. Independent on the degree of mechanical load (polishing < grinding < milling) no decomposition or segregation could be observed. Milling induces a significant increase in disturbance of the crystal structure which can be easily reversed by annealing. Pd_2Ga is inert in H_2 atmosphere against formation of hydrides and starts to oxidize in 20% O_2 atmosphere not below 300 °C.

Table 1: Lattice parameters of Pd_2Ga after grinding (a), milling (b) and milling with subsequent thermal treatment at 400 °C in 5% H_2/Ar (c) as determined by XRD. While no distinctive differences in lattice parameters are observed, after milling, a significant diffraction line broadening (values are given for the 203 reflection) is visible.

Sample preparation	*a*	*b*	*c*	FWHM / °
a)	5.4809(2)	4.0556 (1)	7.7895(1)	0.26
b)	5.4796(2)	4.0599(1)	7.7889 (2)	0.80
c)	5.4815(1)	4.0556(1)	7.7859(1)	0.23

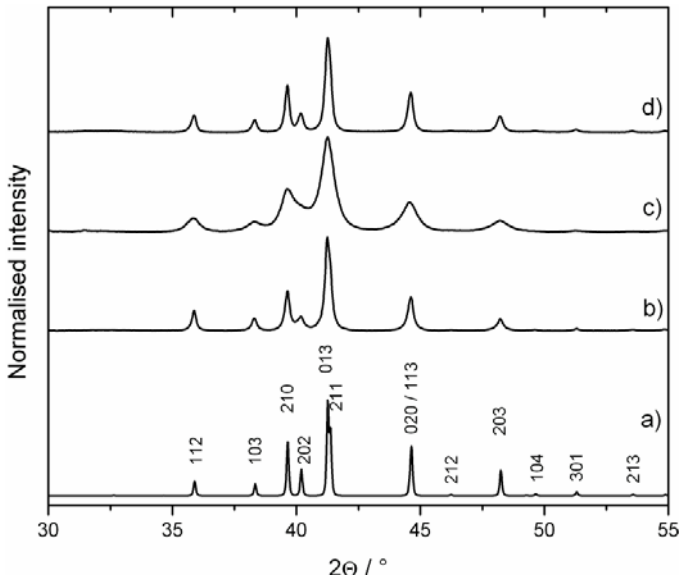

Figure 2: X-ray diffraction patterns of Pd_2Ga after different treatments. a) calculated pattern[41] b) ground c) milled d) milled and subsequently treated 4 h in 5% H_2/Ar at 400 °C.

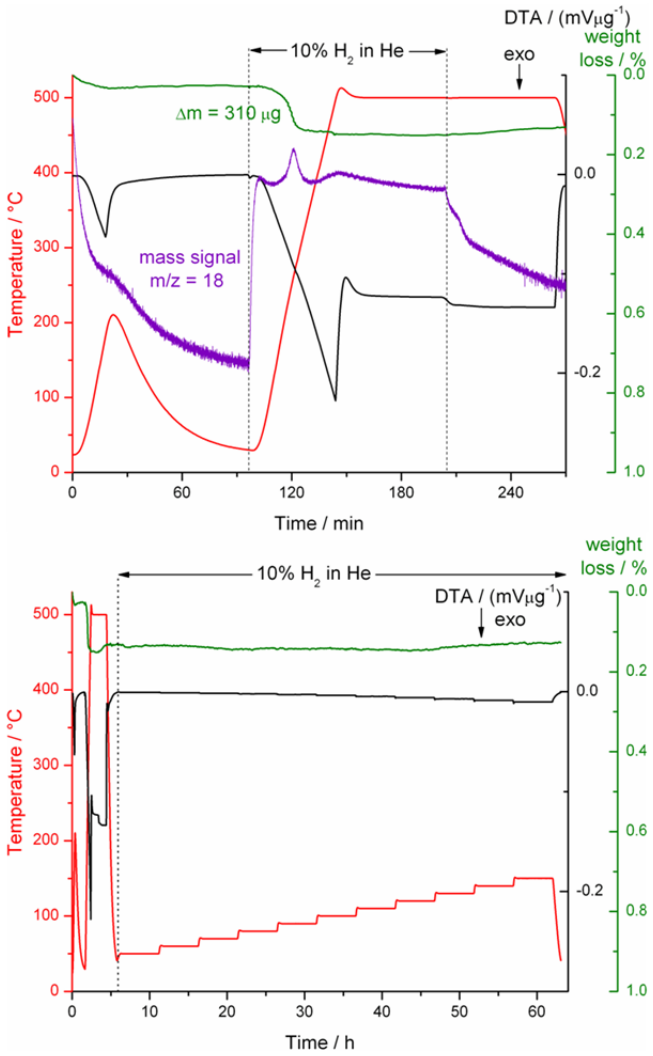

Figure 3: ***In situ*** **DTA/TG/MS measurement of as prepared milled Pd_2Ga. Top: The powder was initially heated in He to 200 °C (10 K/min) to desorb water from the surface. After cooling the atmosphere was changed to 10% H_2/He and the powder was heated to 500 °C (10 K/min) revealing an exothermic peak at 180 °C accompanied by H_2O formation due to surface oxide reduction. Bottom: No further phase transformations were detected also during the long time treatment of the powder in 10% H_2/He with a stepwise increase of the temperature from 50 to 150 °C.**

3.2 Characterization and stability of the surface

To investigate the surface of the Pd_2Ga powder, XPS and high-resolution TEM were applied. XPS is an integral method and provides information about the electronic structure, the chemical composition and the oxidation state of the material in the near-surface region. Using synchrotron radiation with variable photon energies allows measurements at different information depths. On the other hand, HR-TEM gives a complementary and direct local view on the micro- and nano-structure of the surface of the particles.

3.2.1 XPS investigation of the metallographic specimen

Figure 4 represents the Pd 3d core level XP spectra of the as prepared metallographic specimen of Pd_2Ga, which was recorded under UHV and ambient temperature as well as after heating to 400 °C. Additional reference spectra obtained from a Pd foil are also shown. The fits of the specimen heated to 400 °C and the Pd foil are shown in Figure SI 5. An asymmetric Pd $3d_{5/2}$ peak of elemental Pd located at a binding energy of 335.1 eV is observed for the palladium foil in agreement with the literature[59]. On the other hand the Pd $3d_{5/2}$ peak of the Pd_2Ga specimen, heated to 400 °C, is significantly shifted towards a higher binding energy of 336.0 eV (335.9 eV at E_{Kin} = 145 eV) accompanied by a loss of asymmetry. The core-level shift is in agreement with previous results for supported Pd_2Ga[45,46] but - remarkably - as high as reported earlier for the more Ga rich unsupported PdGa sample[34]. We attribute the slightly lower binding energy obtained at the lowest excitation energy (highest surface sensitivity) to a further surface core-level shift. The asymmetry of metallic core levels originates from the probability of excitation of electron-hole pairs at the Fermi level (final state effects)[33,60] and is thus correlated with the number of electronic states at the Fermi level. Figure 5 compares the observed valence bands (with the main contribution of the Pd 4d states) and the Ga 3d core level spectra for the different samples at an excitation energy of 710 eV. Compared to elemental Pd the d-band centre of Pd_2Ga, heated to 400 °C, is significantly shifted away from the Fermi level towards higher binding energies resulting in a lower density of states at the Fermi edge, which is the consequence of intermetallic compound formation and the associated filling of the 4d states of Pd as it was reported for PdGa [34]. The Ga 3d spectra of the Pd_2Ga specimen, heated to 400 °C reveal a doublet at approximately 18.4 and 18.8 eV, which can be assigned to (inter)-metallic Ga[61]. A weak signal at 20.3-20.8 eV corresponds to oxidized Ga, whose atomic proportion increases from ~1 to 9% with decreasing information depth (see Table 2). The ratios of Pd to metallic Ga are

in the range of 2.3-1.6 depending on the kinetic energy of the photons, thus they are close to the stoichiometric composition of 2:1, confirming the presence of an almost clean intermetallic surface under these conditions. In this respect it has to be taken into account, that the quantification using theoretical cross sections is not accurate enough to give a precise absolute ratio of the elements in particular for very low kinetic energies, while relative changes in element ratio of the sample with different information depths or due to changes of the conditions in the XPS chamber can be accurately determined.

The Pd $3d_{5/2}$ peak of the as prepared metallographic specimen (before heating) is still almost symmetric, but broader and was observed at a binding energy of 335.6-335.7 eV (see Figure 4), as it was reported earlier for unsupported Pd_2Ga[40]. It is thus located between that, obtained for elemental Pd and the clean intermetallic surface. This difference is also reflected in the valence band (Figure 5) showing an intermediate structure with an increased density of states close to the Fermi edge. The Ga 3d spectra reveal a significant amount of Ga^{3+} (increasing from ~21 to 60% with increasing surface sensitivity, Table 2). Lower valent $Ga^{\delta+}$ ($0 < \delta < 3$) species were not observed. While the ratio of Pd to the total content of Ga is between 1.7 and 1.6 the ratios of Pd to metallic Ga increases from 2.2 to 4.0 with increasing surface sensitivity. This indicates oxidative decomposition of the IMC resulting in oxidized Ga species and a Pd enriched surface, which must have happened during preparation and/or storing of the sample under Ar atmosphere due to the presence of traces of O_2 and H_2O. The nature of the excess Pd is unclear. In Figure SI 6 we show in detail, that it is not possible to describe the resulting Pd $3d_{5/2}$ peak by a linear combination of the symmetric peak for clean Pd_2Ga and the strongly asymmetric signal for elemental bulk Pd. Additional fit components are necessary to describe the obtained spectra, whose implementation is subjected to a certain arbitrariness due to the peak overlap of the components and the lack of a suitable reference for the unknown structural nature of the formed Pd species. The peak fitting (Figure SI 6) and

the quantification of C 1s (table SI 1) exclude a Pd-C phase, which would also show a Pd 3d peak between those of Pd_2Ga and elemental Pd. We will see in the following sections that this "intermediate" electronic structure of (not too heavily decomposed) samples is variable and depends on the amount of excess Pd. It is plausible that, deviating from the phase diagram[62], the (not necessarily equilibrated) near-surface region of Pd_2Ga is able to accommodate much more Pd, leading to smooth transitions in the electronic and structural state between Pd_2Ga and Pd. Furthermore, it is likely that additional intensity in the Pd 3d spectra originates from the presence of small elemental Pd particles or clusters, giving rise to size-related core-level shift with similar extent as with Pd_2Ga[59]. We will thus restrict the discussion of the Pd 3d spectra in the following on the position and the FWHM of the Pd $3d_{5/2}$ signal, which as a measure of the degree of surface decomposition into oxidized Ga and Ga-depleted Pd. The observed lines will not be fitted due to the questionable reliability of the derived structural data.

Heating of the specimen to 400 °C in dynamic vacuum is sufficient for a re-forming of an IMC terminated surface. An explanation for the high reducing potential of the dynamic vacuum at higher temperatures can be given by analyzing the C1s spectra (Figure SI 7). Before heating, a broad peak at around 284.9 eV is observed indicating the presence of hydrocarbons on the surface, which is an unavoidable feature in our *in situ* XPS chamber. After heating of the specimen, the C 1s signal is weaker and asymmetric and its peak shifts significantly to a lower binding energy of about ~284.2 eV, which is a clear evidence for dehydrogenation of hydrocarbons[63]. Thus, the reduction of the surface Ga oxide in the XPS chamber is likely related to this process.

Table 2: Comparison of peak maxima and FWHM of Pd $3d_{5/2}$ at different kinetic energies: metallographic specimen as prepared (a), metallographic specimen heated to 400 °C in dynamic vacuum (b) and a Pd foil (c). The ratios of Pd and Ga in dependence of the information depth and the amount of oxidized Ga are also given.

	Peak-maximum / eV			FWHM / eV			Pd^{total}:Ga^{total}			Pd^{total}:Ga^{0}			Ga^{3+}:(Ga^{3+}+Ga^{0}) / %		
E_{kin}	785	375	145	785	375	145	785	375	145	785	375	145	785	375	145
a)	335.7	335.7	335.6	1.00	0.96	0.95	1.7	1.6	1.6	2.2	2.7	4.0	21.2	37.8	60.4
b)	336.0	336.0	335.9	0.92	0.85	0.83	2.3	1.6	1.5	2.3	1.7	1.6	1.3	5.8	9.0
c)	335.2	335.1	335.1	1.16	1.02	1.02									

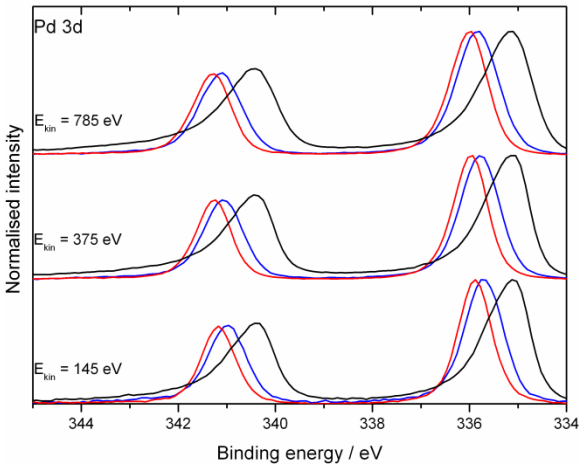

Figure 4: Pd 3d XP spectra of a Pd foil (black) and a metallographic specimen (polished under Ar) in an as prepared state (blue) and after thermal treatment at 400 °C in dynamic vacuum (red).

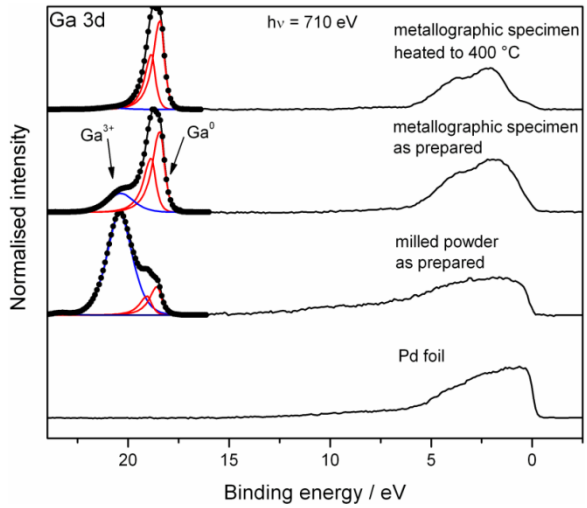

Figure 5: Ga 3d and valence spectra of different Pd_2Ga samples. The change of the valence band structure with the amount of oxidized Ga is obvious.

3.2.2 XPS and HR-TEM investigations of milled Pd_2Ga in the as prepared state

The Pd 3d XP spectrum of milled Pd_2Ga is shown in Figure 6. A very broad and asymmetric peak indicates a decomposition of the intermetallic compound at the surface to a large extent. The asymmetric peak shape and the shift of the peak position to lower binding energies with increasing surface sensitivity from 335.5 to 335.2 eV indicates that mainly elemental Pd is present at the decomposed surface. In the most surface sensitive Pd 3d spectrum a long tail of the peak to higher binding energies represents undefined species, which are probably due to oxidized Pd species[64]. It is noted that also intermetallic Pd-Ga compounds with a higher Ga content show peaks at similar positions, but these are unlikely to co-exist with oxidized Ga at the surface. Finally, charging effects might additionally broaden the line shape and residues of intermetallic Pd_2Ga likely also contribute to the spectra as indicated by the small contribution of (inter)-metallic Ga, visible in the Ga 3d spectra in Figure 5. The total Pd:Ga ratio shows a vast excess of Ga (Table 3), which probably origins from segregation of Ga due to oxidation during the mechanical treatment. However, most of the Ga is oxidized and the ratio between Pd and metallic Ga is by far higher than the nominal composition 2:1 showing that the oxidation of Ga species leaves a Ga-depleted Pd phase at the surface of the Pd_2Ga particles. Accordingly, the valence band (Figure 5) of as prepared milled Pd_2Ga clearly resembles that of elemental Pd and not that of clean Pd_2Ga recorded after heating of the metallographic specimen.

In contrast to the metallographic sample, for milled powder the reducing potential in the XPS chamber or the amount of reducing carbonaceous deposits is not sufficient for a complete reduction of the thick surface oxide layer to reform the intermetallic Pd_2Ga. The high temperature treatment at 400 °C in dynamic vacuum leads to a shift of the Pd $3d_{5/2}$ peak to 335.7 eV, which becomes nearly symmetric but shows still an enhanced broadness. After air exposure for 10 min the sample was measured again. The Ga oxide content increases slightly

without observing a shift of the Pd 3d peaks. After storing the sample two months under air no further changes in XP spectra of Ga 3d and Pd 3d could be observed, indicating that the surface readily passivates without further mechanical load and the associated energy input.

HR-TEM images of the Pd_2Ga particles (Figure 7) provide a closer look on the local structure and morphology of the surface of the particles. The bulk of the material consists of crystalline Pd_2Ga particles, which is in agreement with the XRD result. The particles are surrounded by a non-uniform amorphous over-layer, which - according to XPS - mainly consists of oxidized Ga species. In this over-layer, crystalline nanoparticles with a diameter of up to 5 nm are embedded and in some case elemental Pd as well as Pd_2Ga could be unambiguously identified. However, Pd and Pd_2Ga cannot be easily distinguished by the diffraction pattern even in atomic resolution TEM because of the close relation of the structures[43].

Table 3: Comparison of peak maxima and FWHM of Pd $3d_{5/2}$ at different kinetic energies: milled powder as prepared (a), powder heated to 400 °C in dynamic vacuum (b). Quantification of Pd and Ga always shows a large excess of Ga. Due to the high content of oxidized Ga the surface is enriched on Pd with respect to the present metallic Ga.

	Peak-maximum / eV			Peak-FWHM / eV			Pd^{total}:Ga^{total}			Pd^{total}:Ga^{0}			Ga^{3+}:(Ga^{3+}+Ga^{0}) %		
E_{kin}	785	375	145	785	375	145	785	375	145	785	375	145	785	375	145
a)	335.5	335.4	335.2	1.32	1.24	n.d.	1.0	0.9	0.6	4.5	7.4	29.8	78.0	88.1	97.9
b)	335.7	335.6	335.6	1.13	1.06	1.05	1.3	1.5	1.4	2.1	2.7	3.0	33.6	46.7	55.6

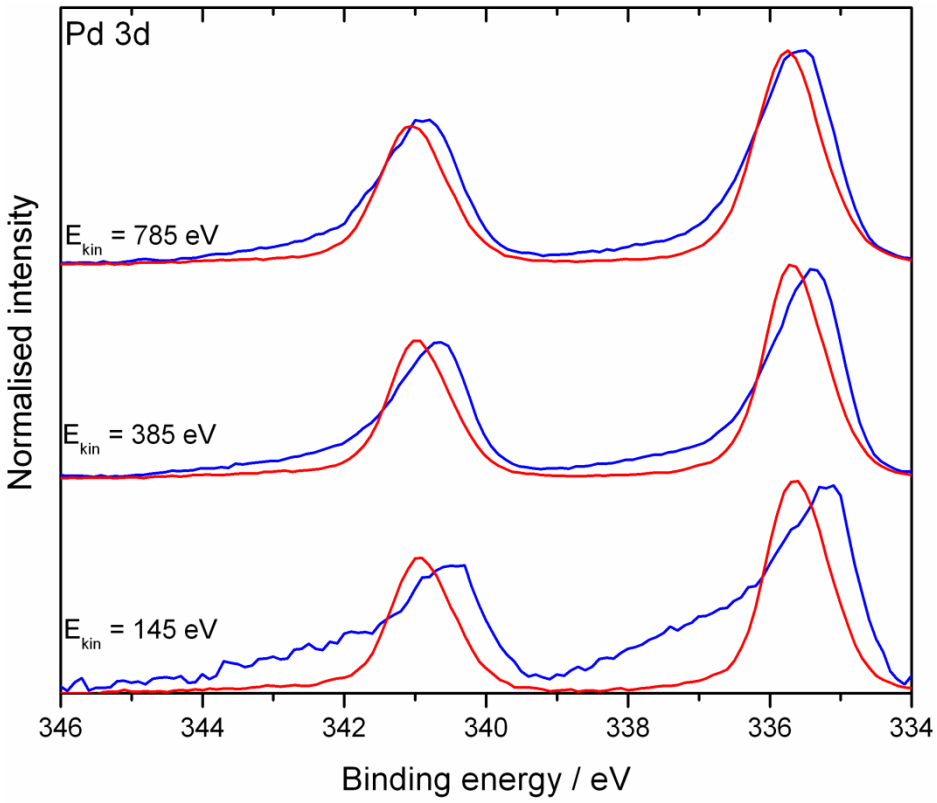

Figure 6: Pd 3d depth profiling of milled Pd_2Ga in an as prepared state (blue) and heated to 400 °C (red).

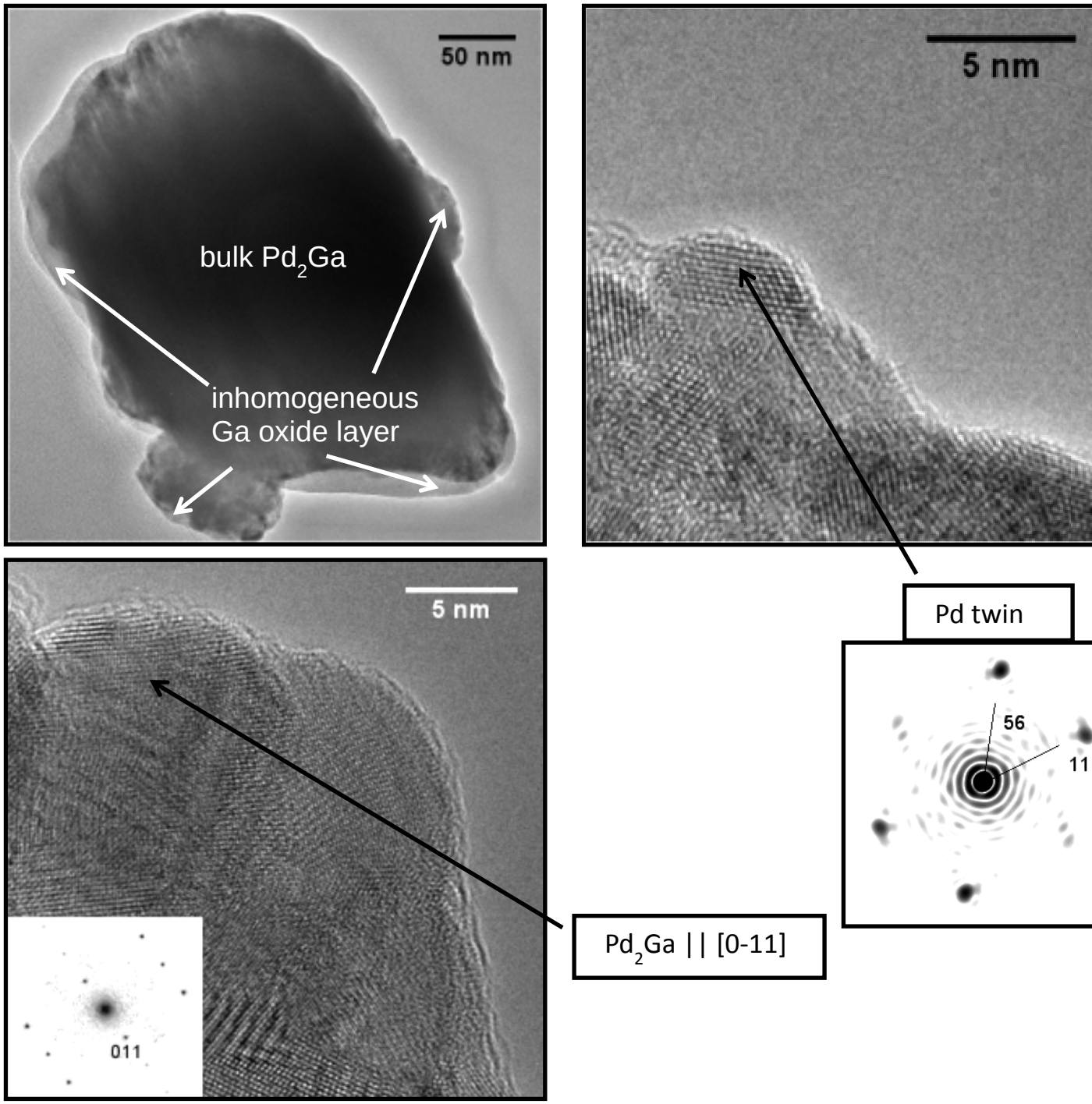

Figure 7: HR-TEM of milled Pd_2Ga in an as-prepared state. Large crystalline Pd_2Ga particles are surrounded by an inhomogeneous amorphous Ga oxide layer. At certain parts of the layer nanoparticles are embedded.

3.2.3 XPS and HR-TEM investigations of ex situ pre-reduced milled Pd_2Ga

Because the maximum H_2 pressure in the XPS chamber is limited to ~1 mbar and a full reduction of a thick oxide layer was not possible under these conditions, two *ex situ* pre-reduced samples (5% H_2/Ar, 1 bar total pressure, 4 h, 400 °C) were transferred under Ar into the XPS chamber. The reduction temperature was clearly higher than the reduction peak observed in the DTA/TG/MS measurement (Figure 3) with an onset temperature of 180 °C which was assigned to the reduction of the surface oxide layer. The higher temperature allows also a structural healing of the intermetallic surface. One sample was cooled down in Ar after reduction, the other one was cooled down in 5% H_2/Ar. In both cases the surface stoichiometry is close to the nominal composition of 2:1 (Table 4), which can be explained by the absence of any mechanical treatment after high-temperature reduction and, as will be shown below, by a mild passivation process. In the latter sample only about 20% Ga are in an oxidized state (on the most surface sensitive XPS measurement, see Figure 9 b) and the Pd $3d_{5/2}$ peak is located at 335.85 eV. Apparently this thin passivation layer is unavoidable if the environment falls below a certain reduction potential. The reason therefore is likely the uncoordinated sites at the outermost surface with reduced covalent stabilization, which are extremely reactive towards oxygen impurities. *In situ* H_2 treatment of the sample, leading to the reduction of the surface Ga oxide (see Table 4, Figure 9), indicate no further shift or change in peak shape and width of the Pd 3d peak and also the valence band structure remain unaltered. This implies that the slightly lower binding energy (compared to 336.0 eV in the more bulk sensitive measurements, compare Table 2) originates from a surface core-level shift, rather than the influence of an overlapping Pd component. However, the presence of 20% Ga oxide before *in situ* reduction must involve a Ga-depletion of the remaining Pd near-surface species. On the one hand, Pd_2Ga provides a certain homogeneity range and the formed Ga oxide passivation layer could originate from segregation from the subsurface or

the bulk and thus the IMC might balance this loss of metallic Ga. On the other hand, if Ga from the outermost Pd_2Ga layers is oxidized this would leave behind very small Pd accumulations. As already discussed, small Pd clusters might provide a rather similar electronic structure compared to Pd_2Ga[59]. Furthermore it is clearly visible in Figure SI 6, that also small concentrations of bulk Pd (~1%) are hardly detectable by XPS in our case. Thus, small amounts of elemental Pd are likely to be still present.

The surface is more decomposed, if the sample is cooled in the absence of H_2 under 100% Ar atmosphere (O_2 and H_2O concentration < 100 ppb) after the *ex situ* pre-reduction. It results in a stronger oxidation of about 75% of Ga (Figure 9 a) and a slightly asymmetric Pd $3d_{5/2}$ peak is observed at 335.5 eV (see Figure 10). This intermediate core level shift is lower than observed for the as prepared metallographic specimen or the milled sample heated to 400 °C. That lower core level shift is consistent with the larger excess of Pd compared to metallic Ga (7.5:1) but eludes again a reference-based fitting analysis. The difference of the electronic structure is also clearly visible by the different valence band features (see Figure 8 b and c). Cooling a pre-reduced sample in Ar, results already in a higher occupation of the d-band close to the Fermi level. These differences strikingly clarify the sensitivity of the intermetallic surface towards oxidative decomposition once the temperature is high and the reducing potential of the environment is not sufficient to outweigh the oxophilicity of the surface Ga species even under condition where gas phase O_2 or H_2O are present only on a minimum impurity level.

The corresponding HR-TEM images (Figure 11) of the pre-reduced particles cooled down in 5% H_2/Ar show again crystalline particles consisting of Pd_2Ga in the bulk which is surrounded by a thinner and more uniform amorphous layer.

3.2.4 *In situ* H_2 treatment of pre-reduced milled Pd_2Ga and re-oxidation

Treatment in 1 mbar H_2 at 400 °C in the XPS chamber allows removing the oxide layers almost completely from both (cooled in 5% H_2/Ar and in 100% Ar) *ex situ* pre-reduced samples (Figure 9 c). Henceforth also the sample cooled down in 100% Ar provides the electronic structure of Pd 3d core level (Figure 10) and valence band (Figure 8 e) of pure Pd_2Ga at the surface. However, analyzing the ratio between Pd and Ga both samples are subjected to variations of their surface stoichiometry. The Ar-cooled sample shows an increase of the Pd:Ga ratio to about 2.8 at 400 °C in 1 mbar H_2 and a pronounced decrease to 0.9 when changing to 50 °C in UHV. The H_2-cooled sample also shows a by far too low ratio of about 1.2, in this case even at 400 °C in 1 mbar H_2 atmosphere. These changes are not associated with variations of the Pd 3d peak profile or position, which excludes the formation of more Ga rich or Ga less near-surface alloys. For the latter sample the ratio between Pd and the total content of Ga was much higher at 1.7 when the spectra were recorded at higher kinetic energies of 375 or 785 eV. Because the binding energy of elemental, polycrystalline Ga is very similar to intermetallic Ga[65] and the resolution of the Ga 3d peaks is not sufficient to distinguish between both, segregation of elemental Ga to the surface is the most likely explanation. However, the ratio stays constant near 1:1 even after abrupt exposure and store of 5 h in air. Since this phenomenon is only observed after reduction in the XPS chamber under reduced pressure and not after *ex situ* pre-reduction, we currently have no explanation for this observation and speculate that this manifestation of dynamic behavior is caused by the special low-pressure conditions in the XPS chamber.

The general sensitivity of the surface redox processes of Pd_2Ga on the exact conditions and the dependence of its reversible character on the sample history is also observed during re-oxidation. If the sample without a protecting oxide-layer is abruptly exposed to air, the amount of oxidized Ga increases to more than 40% and the peak shape of Pd 3d changes and

loses its narrow and symmetric profile (Figure 10). It is indeed the sole exception, where the observed line profile can approximately be described by a linear combination of 80% Pd_2Ga and 20% bulk Pd (Figure 6 d) evidencing the formation of elemental Pd as it was already assumed by Haghofer et al.[47]. The situation is different if the sample is carefully oxidized. Slow *in situ* treatment with a step-wise increase of O_2 and H_2O (ratio ~ 1:1) partial pressure up to 0.6 mbar total pressure at 40 °C within some hours resulted in oxidation of only approximately 25% of Ga at the outermost surface, which is not accompanied with a significant d-band shift or increase in FWHM of the Pd3d peak (Figure 10) and a subsequent air-exposure did not lead to further oxidation indicating the formation of a thin passivation layer by very slow oxidation.

Table 4: Peak position and FWHM of Pd $3d_{5/2}$ and elemental quantification of Pd and Ga and Ga oxide content of *ex situ* pre-reduced milled Pd_2Ga recorded at a kinetic energy of 145 eV. a) sample cooled down under 100% Ar, b) in situ H_2 treatment (1 mbar) of the sample of a) at 400 °C, c) sample of b) after slow *in situ* oxidation and subsequent exposure to air, d) *ex situ* pre-reduced and cooled down under 5% H_2/Ar, e) *in situ* H_2 treatment (1 mbar) of samples of d) at 400 °C, f) sample of e) after abrupt exposure to air (2 signals).

	Peak-maximum / eV	Peak-FWHM / eV	Pd^{total}:Ga^{total}	Pd^{total}:Ga^0	Ga^{3+}:(Ga^{3+}+Ga^0) %
a)	335.50	1.07	1.9	7.5	74
b)	335.85	0.85	2.8	2.9	4
c)	335.85	0.79	0.7	0.96	27
d)	335.85	0.82	2.1	2.7	19
e)	335.85	0.85	1.2	1.2	4
f)	335.9 and 335.1	0.85 and 1.0	1.0	1.7	42

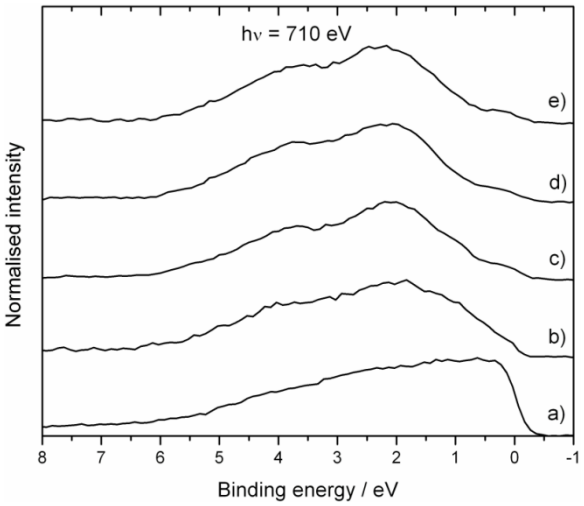

Figure 8: XP spectra of the valence band at a photon energy of 710 eV. a) Pd foil b) *ex situ* pre-reduced milled powder and cooled under Ar c) *ex situ* pre-reduced milled powder cooled under H_2 d) metallographic specimen heated to 400 °C and e) sample of b) during treatment in 1 mbar H_2 at 400 °C.

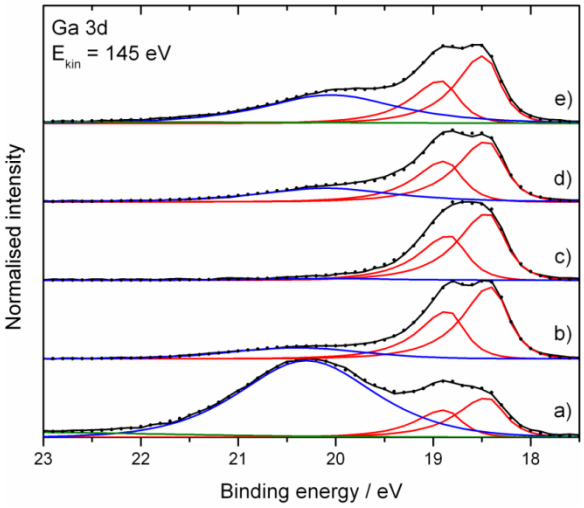

Figure 9: Ga 3d spectra of different pre-reduced Pd_2Ga powder samples. a) *ex situ* pre-reduced powder, cooled under Ar b) *ex situ* pre-reduced cooled under H_2 c) *in situ* H_2 treatment after ex situ pre-reduction and cooling under Ar d) sample of c) after slow oxidation in the cell and subsequent air exposure e) sample of c) after abrupt exposure to air. Red lines represent fits of the intermetallic Ga 3d doublet while blue lines correspond to oxidized Ga species. In the case of a high oxidation grade also a broad signal of O 2s (green) is observed ~ 23 eV.

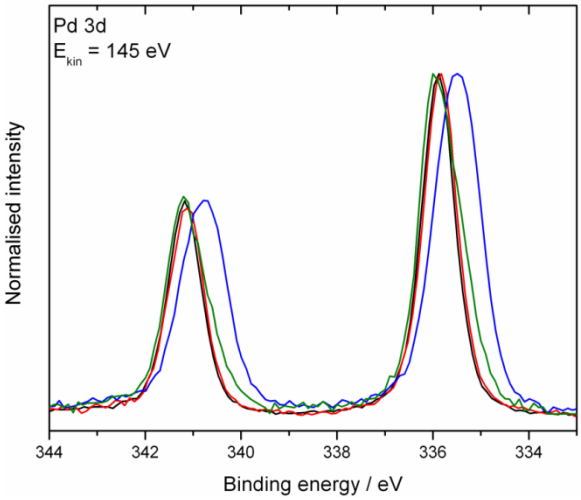

Figure 10: Pd 3d spectra of *ex situ* pre-reduced powders at a kinetic energy of 145 eV. The red curve represents the *ex situ* pre-reduced milled powder cooled under 5% H_2/Ar and is almost similar to the metallographic specimen heated to 400 °C (black curve) and the samples treated *in situ* with H_2 at 1 mbar (not shown). *Ex situ* pre-reduction and cooling under 100% Ar leads to significant disruption of the surface (blue curve) as well as the abrupt exposure to air of an freshly reduced sample (green).

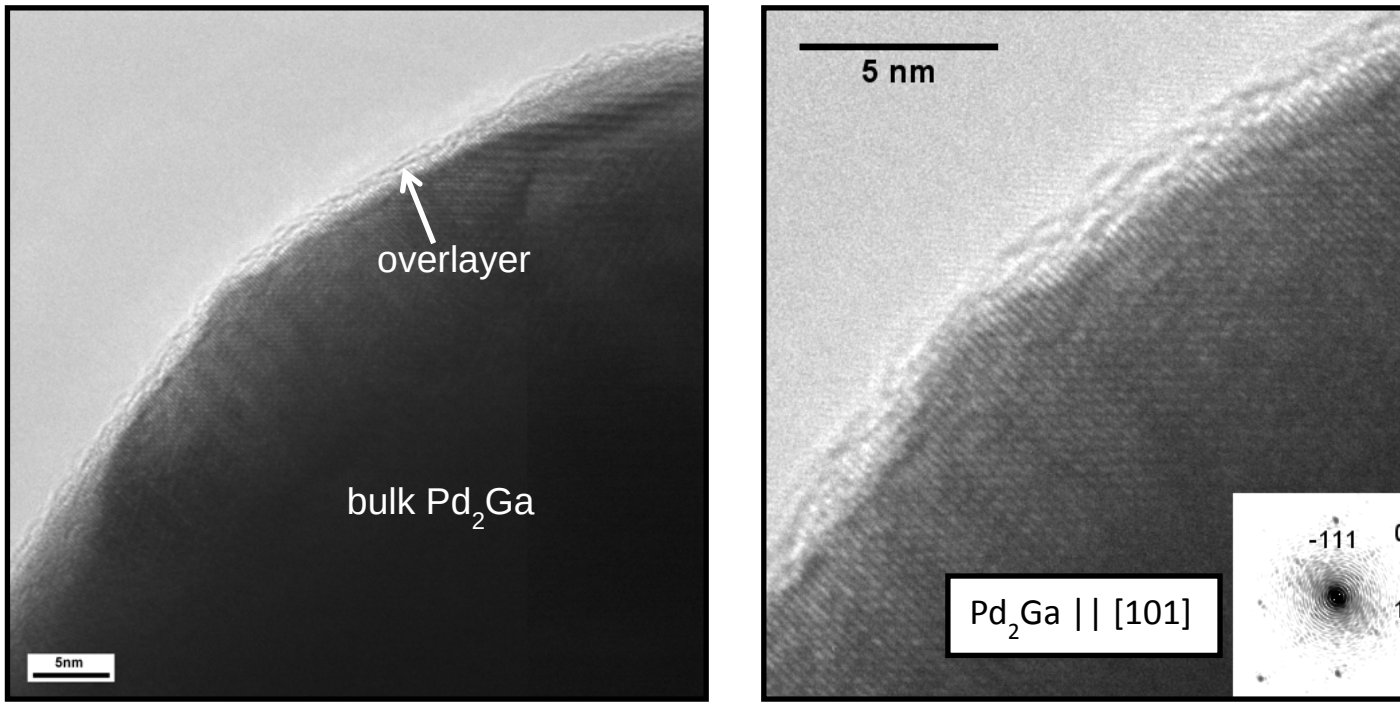

Figure 11: HR-TEM of Pd_2Ga powder after pre-reduction at 400 °C. These particles consist of large domains and are surrounded only by a thin amorphous over-layer. Beside possible contaminations in the microscope, according to the XP spectra Ga oxide contribute to the thin over-layer.

4. Summary

In this study we investigated the bulk and the surface stability of the intermetallic compound Pd_2Ga. The bulk of Pd_2Ga provides a high chemical stability. Pd_2Ga is inert against hydride formation at low as well as at high temperatures. Oxidative decomposition of the bulk is not observed before ~ 300 °C in 20% O_2/Ar atmosphere. The bulk material is furthermore highly resistant against mechanical load and remains single phase material even after milling. The induced strain effects are easily reversible by a temperature treatment at 400 °C. These observations are in agreement with the results for PdGa and Pd_3Ga_7. However, the high stability of the bulk of Pd_2Ga cannot be transferred to the surface. The dynamics of the surface are complex and depend on the pre-treatment and the actual conditions, which is summarized in Figure 12. A metallographic specimen was introduced as reference sample for the XPS studies. The polishing and subsequent storage of this sample under Ar atmosphere at room temperature is already sufficient for partial oxidative decomposition resulting in a Pd enriched metallic state partially covered by Ga oxide (Figure 12 A). According to the XPS analysis small Pd accumulations, rather than bulk Pd is present. These Pd particles likely act as nuclei for the re-formation of the IMC at the surface by annealing of the specimen to 400 °C in dynamic vacuum (Figure 12 B). The Ga oxide reduction is likely assisted by a Pd induced dehydrogenation of hydrocarbon surface impurities in the XPS chamber resulting in carbonaceous species at the surface. Mechanical load during milling leads to enhanced surface segregation and oxidation of Ga. The surface of an air-milled sample is nanostructured and consists of Pd, Pd oxide and Pd_2Ga nanoparticles embedded in an inhomogeneous Ga oxide layer (Figure 12 C). The annealing to 400 °C in dynamic vacuum is not sufficient for a complete re-formation of the IMC at the surface (Figure 12 D), whereas under atmospheric pressure the oxide over-layer reduces at 180 °C in 10% H_2/He. The powder was thus (with regard to its application in liquid phase hydrogenation, see part II[50])

ex situ pre-reduced at 400 °C in 5% H_2/Ar and, presumably, under these conditions the surface is a clean termination of the bulk (Figure 12 E). After cooling the sample under this reducing atmosphere and careful handling under Ar we observed the Pd 3d core level as well as the valence band spectra compatible with that of the clean intermetallic surface within the detection limit (Figure 12 F). However, a thin passivation layer is unavoidable due to the structural destabilization of Pd_2Ga – likely a consequence of the uncoordinated Ga sites of the termination layer. According to previous literature[47,48] and our observed activity in hydrogenation, presented in part II of this work[50], we suggest that the oxide layer is not homogeneous. It is possible that Pd_2Ga tolerates some loss of the metallic Ga, due to its homogeneity range, but traces of elemental Pd could still be present. The situation is much clearer, when the sample is cooled under Ar after reduction (Figure 12 G): in absence of H_2 at high temperature smallest traces of O_2 or H_2O are enough for strong decomposition and segregation of the surface even in absence of mechanical load. The *in situ* H_2 treatment *under low pressure conditions* of these samples lead to dynamic enrichment of metallic Ga on top of the surface, apparently without the formation of a more Ga rich IMC, e.g. PdGa (Figure 12 H). The mechanism of this process is unclear, but possibly it is an equilibration of the IMC terminated surface. However, despite the Ga enrichment, different surfaces were observed after oxidative treatments (Figure 12 I and J): If the material is suddenly exposed to air, this resulted indeed in the partial formation of metallic Pd. In the case of careful, slow oxidization at room temperature under reduced pressure only a thin Ga oxide layer is formed. This passivation layer does not grow after air exposure and, within the detection limit, no further disturbance of the under-lying IMC was observed.

The surface of Pd_2Ga turned out to be highly dynamic. A passivation layer forms rapidly as soon as the environment loses a certain reduction potential. The stability of the passivation layer and the degree of disturbance of the (electronic) structure of the surface strongly

depends on the pre-treatment and the environment, i.e. mechanical load, partial pressure of oxidants, total pressure and temperature. Thus the behavior of the intermetallic Ga in Pd_2Ga is comparable to pure elements with high oxophilicity like elemental Ga, Al, Zn or Ti where a passivating layer is rapidly formed without further attack of the bulk. In sharp contrast to the pure elements, the oxidized over-layer of Pd_2Ga can be removed by reduction in hydrogen at relatively low temperatures, which is likely an effect of the presence of finely dispersed excess Pd, which activates H_2 by dissociative chemisorption. The exact nature of the excess Pd could in most instances not be clarified in this study and depends presumably also on the pre-treatment. The presence of Pd enriched phases with intermediate electronic and structural state between Pd and Pd_2Ga could explain the observations. Furthermore, it is likely that small Pd agglomerates with a small size distribution are formed on the surface which are partially embedded in a Ga oxide matrix. Their spectroscopic motifs (core level shift, reduced density of states at the Fermi level) are compatible with the observations and are unfortunately largely indistinguishable from Pd_2Ga itself[59]. It can be assumed that the catalytic properties of decomposed Pd_2Ga surfaces are dominated by this segregated Pd species rather than by the IMC itself.

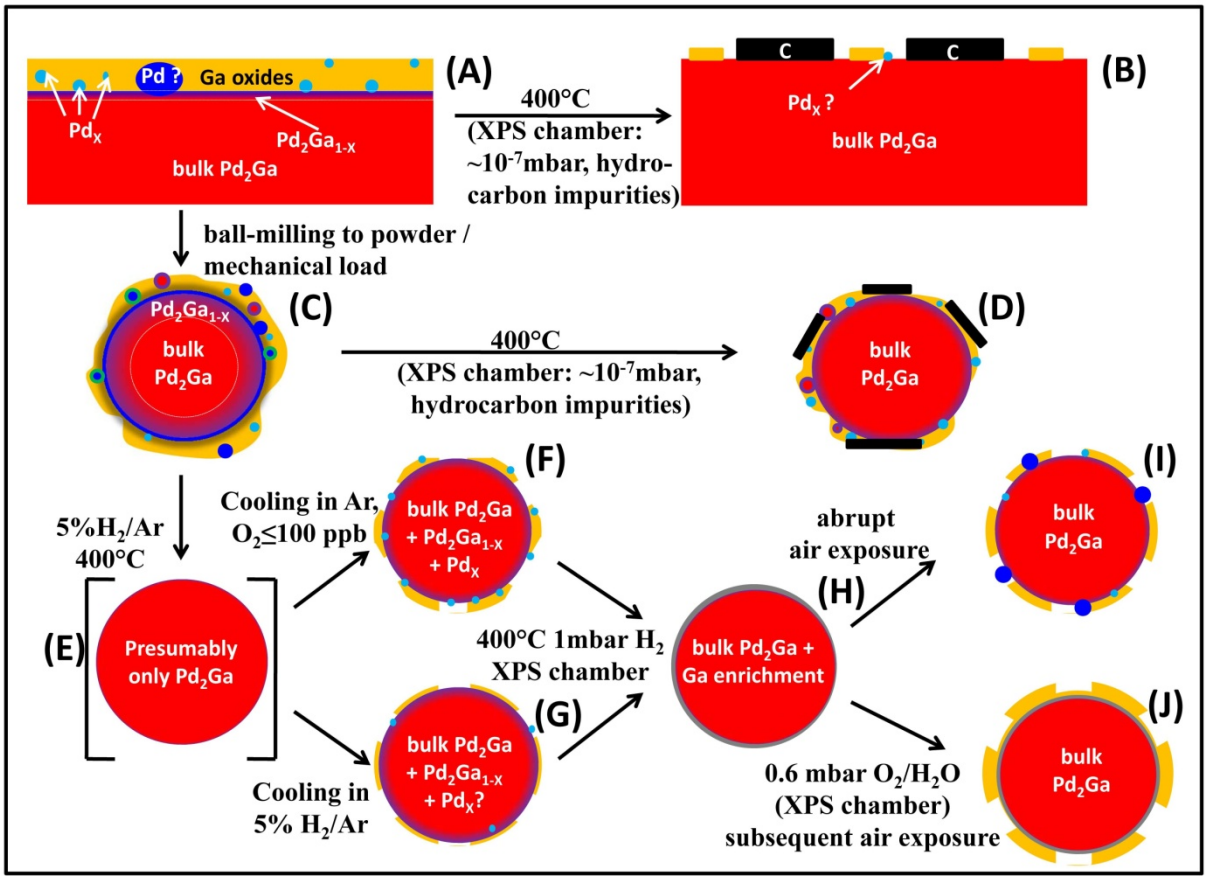

Figure 12: Scheme of the observed dynamic changes of Pd_2Ga after different treatments. The rectangle shown in (A) and (B) indicate the metallographic specimen. The spherical sketches (C-J) represent a microcrystalline particle after milling. The non-uniform morphologies and distribution of the nanostructures in particular that of the smaller Pd agglomerates (Pd_X, light blue), larger metallic Pd accumulations (dark blue), Pd oxide (green) and C accumulations (black) at the surface are simplified. The bulk of Pd_2Ga (red areas) is always stable. Ga oxide is shown in yellow color. A layer of varying thickness at the interface of the bulk and the Ga oxide, shown in purple, marks slightly Pd enriched Pd_2Ga due to Ga surface segregation. The grey cover visible in (H) should indicate the irreversible enrichment of metallic Ga on top of the surface during *in situ* H_2 treatment in the XPS chamber.

5. Conclusion

Our study represents a detailed investigation of the surface stability of the Pd_2Ga, which shows high selectivity in the hydrogenation of acetylene in the gas phase as previously reported. Pd and Ga are chemically very different metals and the reaction between both results in the formation of covalent bonds. Contrariwise to alloys, the covalent bonds strongly alter the crystal and the electronic structure. Compared to elemental Pd, the valence band of Pd-Ga intermetallic compounds possesses a structure comparable to a coinage metal with a

clear shift of the d-band center away from the Fermi level. These covalent bonds between Pd and Ga, however, are not strong enough to stabilize the material's surface against oxidizing agents and against mechanical load. If the reduction potential falls below a certain value, a passivating over-layer forms and the surface becomes chemically different. The bulk however is protected against further decomposition. The electronic structure of the surface is subjected to a high dynamics with respect to the pre-treatment of the material and the chemical environment. The reason for the reversible character of these disturbances is the formation of metallic Pd accessible to the surface with its ability to activate hydrogen. However, this shows that it is not sufficient to determine the electronic structure and the composition of a freshly prepared intermetallic surface under clean or reducing conditions, since during sample preparation before reaction or under reaction conditions this surface can and will easily change. The termination of the surface may differ substantially from a cut through bulk structure, even if bulk methods still confirm the presence of the intermetallic compound. The impact of this issue for catalytic reactions will be addressed in part II of this study[50] by means of the liquid phase hydrogenation of phenylacetylene catalyzed by Pd_2Ga. The discrepancy between surface and bulk with a dynamic behavior that is dependent on the chemical potential of the environment is a manifestation of the well-known materials and pressure gaps that hinder straightforward correlation of structural analysis obtained on model systems with catalytic performance data. It is perspicuous, that these difficulties, demonstrated here by means of Pd_2Ga, must be considered when investigating the bulk and surface structure of other intermetallic compounds containing less noble metals.

Acknowledgement

The authors thank Ulrich Burkhardt, Monika Eckert and Gisela Weinberg for the metallographic and microscopic analysis, Horst Borrmann, Yuri Prots and Steffen Hückmann for the XRD measurements and Axel Knop-Gericke and Dirk Rosenthal for the fruitful

discussions concerning the photo electron spectroscopy. We thank the Helmholtz-Zentrum Berlin for providing the beam time and for the continuous support. Timur Kandemir, Edward Kunkes and Yuan Luo are acknowledged for the support during laboratory work.

[1] H. Arnold, F. Döbert, J. Gaube, in: G. Ertl, H. Knözinger, F. Schüth, J. Weitkamp (Eds.), Handbook of Heterogeneous Catalysis, Weinheim, Wiley-VCH, 2008, p. 3271.
[2] V. V. Rusak, M. I. Zaretskii, A. S. Mozzhukhin, I. V. Usyshkina, L. A. Pushkina, Russ. J. Appl. Chem. 67 (1995) 1066.
[3] P. Mercier, P. Chabardes, Pure & Appl. Chem. 66 (1994) 1509.
[4] J. Sobczak, T. Bolesławska, M. Pawłowska, W. Palczewska, Stud. Surf. Sci. Catal. 41 (1988) 197.
[5] G. C. Bond, D. A. Dowden, N. Mackenzie, Trans. Faraday Soc. 54 (1958) 1537.
[6] P. B. Wells, Chem. Ind. (Lond.) (1964) 1742.
[7] G. C. Bond, P. B. Wells, Adv. Catal. 15 (1964) 205.
[8] S. Nishimura, Handbook of Heterogeneous Catalytic Hydrogenation for Organic Synthesis Wiley-Interscience, New York, 2001, p. 148.
[9] A. Borodzinski, G. C. Bond, Catal. Rev. 48 (2006) 91.
[10] Á. Molnár, A. Sárkány, M. Varga, J. Mol. Catal. A 173 (2001) 185.
[11] W. M. H. Sachtler, in: G. Ertl, H. Knözinger, F. Schüth, J. Weitkamp (Eds.), Handbook of Heterogeneous Catalysis, Weinheim, Wiley-VCH, 2008, p. 1585.
[12] V. Ponec, W. M. H. Sachtler in: J. W. Hightower (Ed.), Proceedings of 5th International Congress on Catalysis, Amsterdam, 1972, p. 6541.
[13] M. García-Mota, B. Bridier, J. Pérez-Ramírez, N. López, J. Catal. 273 (2010), 92.
[14] F. D. Manchester, A. San-Martin, J. M. Pitre, J. Phase Equilib. 15 (1994) 62.
[15] A. M. Doyle, S. K. Shaikhutdinov, H.-J. Freund, J. Catal 223 (2004) 444.
[16] A. M. Doyle, S. K. Shaikhutdinov, S. D. Jackson, H.-J. Freund, Angew. Chem. Int. Ed. 42 (2003) 5240.
[17] N. A. Khan, S. Shaikhutdinov, H.-J. Freund, Catal. Lett. 108 (2006) 159.
[18] D. Teschner, Z. Révay, J. Borsodi, M. Hävecker, A. Knop-Gericke, R. Schlögl, D. Milroy, S. D. Jackson, D. Torres, P. Sautet, Angew. Chem. Int. Ed. 47 (2008) 9274.

[19] F. Studt, F. Abild-Pedersen, T. Bligaard, R. Z. Sørensen, C. H. Christensen, J. K. Nørskov, Science 320 (2008) 1320.
[20] D. Teschner, E. M. Vass, M. Hävecker, S. Zafeiratos, P. Schnörch, H. Sauer, A. Knop-Gericke, R. Schlögl, M. Chamam, A. Wootsch, A. S. Canning, J. J. Gamman, S. D. Jackson, J. McGregor, L. F. Gladden, J. Catal. 242 (2006) 26.
[21] D. Teschner, J. Borsodi, A. Wootsch, Zs. Révay, M. Hävecker, A. Knop-Gericke, S. D. Jackson, R. Schlögl, Science 320 (2008) 86.
[22] C. N. Thanh, B. Didillon, P. Sarrazin, C. Cameron, US patent 6054409 (2000), to Institut Francais du Petrole
[23] A. Pachulski, R. Schödel, P. Claus, Appl. Catal. A: General 445–446 (2012) 107.
[24] H. Lindlar, Helv. Chim. Acta 35 (1952) 446.
[25] N. Semagina, M. Grasemann, N. Xanthopoulos, A. Renken, L. Kiwi-Minsker, J. Catal. 251 (2007) 213.
[26] S. Nishimura, Handbook of Heterogeneous Catalytic Hydrogenation for Organic Synthesis Wiley-Interscience, New York, 2001, p. 601.
[27] T. Mallat, A. Baiker, Appl. Catal. A 200 (2000) 3.
[28] N. López, C. Vargas-Fuentes, Chem. Commun. 48 (2012) 1379.
[29] G. Vilé, B. Bridier, J. Wichert, J. Pérez-Ramírez, Angew. Chem. Int. Ed. 51 (2012) 8620.
[30] J. Sobczak, W. Palczewska, T. Boleslawska, M. Pawlowska, Stud. Surf. Sci. Catal. 41 (1988) 197.
[31] H. C. de Jongste, V. Ponec, Bull. Soc. Chim. Belg. 88 (1979) 453.
[32] J. C. Fuggle, F. U. Hillebrecht, R. Zeller, Z. Zołnierek, P. A. Bennett, Phys. Rev. B 27 (1983) 2145.
[33] F. U. Hillebrecht, J. C. Fuggle, P. A. Bennett, Z. Zołnierek, Phys. Rev. B 27 (1983) 2179.
[34] K. Kovnir, M. Armbrüster, D. Teschner, T. V. Venkov, F. C. Jentoft, A. Knop-Gericke, Yu. Grin, R. Schlögl, Sci. Technol. Adv. Mater. 8 (2007) 420.
[35] J. Osswald, R. Giedigkeit, R. E. Jentoft, M. Armbrüster, F. Girgsdies, K. Kovnir, T. Ressler, Yu. Grin, R. Schlögl, J. Catal. 258 (2008) 210.
[36] J. Osswald, R. Giedigkeit, R. E. Jentoft, M. Armbrüster, F. Girgsdies, K. Kovnir, T. Ressler, Yu. Grin, R. Schlögl, J. Catal. 258 (2008) 219.
[37] B. H. Verbeek, P. K. Larsen, W. M. Gerits, Vacuum 33 (1983) 813.

[38] M. Klanjŝek, A. Gradiŝek, A. Kocjan, M. Bobnar, P. Jegliĉ, M. Wencka, Z. Jagliĉić, P. Popčević , J. Ivkov, A. Smontara, P. Gille, M. Armbrüster, Yu. Grin, J. Dolinšek, J. Phys-Condens. Mat. 24 (2012) 085703.
[39] M. Armbrüster, H. Borrmann, M. Wedel, Yu. Prots, R. Giedigkeit, P. Gille, Z. Kristallogr. - New Cryst. Struct. 225 (2010) 617.
[40] K. Kovnir, D. Teschner, M. Armbrüster, P. Schnörch, M. Hävecker, A. Knop-Gericke, Yu. Grin, R. Schlögl, Bessy Highlights 2007 (2008) 22.
[41] K. Kovnir, M. Schmidt, C. Waurisch, M. Armbrüster, Yu. Prots, Yu. Grin, Z. Kristallogr. - New Cryst. Struct. 223 (2008) 7.
[42] H. W. King, F. D. Manchester, J. Phys. F 8 (1978) 15.
[43] C. Wannek, B. Harbrecht, J. Alloys Comp. 316 (2001) 99.
[44] M. Armbrüster, K. Kovnir, M. Behrens, D. Teschner, Yu. Grin, R. Schlögl, J. Am. Chem. Soc. 132 (2010) 14745.
[45] A. Ota, M. Armbrüster, M. Behrens, D. Rosenthal, M. Friedrich, I. Kasatkin, F. Girgsdies, W. Zhang, R. Wagner, R. Schlögl, J. Phys. Chem. C 115 (2011) 1368.
[46] A. Haghofer, K. Föttinger, F. Girgsdies, D. Teschner, A. Knop-Gericke, R. Schlögl, G. Rupprechter, J. Catal. 286 (2012) 13.
[47] A. Haghofer, K. Föttinger, M. Nachtegaalm, M. Armbrüster, G. Rupprechter, J. Phys. Chem. C 116 (2012) 21816.
[48] R. Leary, F. de la Peña, J. S. Barnard, Y. Luo, M. Armbrüster, R. Schlögl, J. M. Thomas, P. A. Midgley, ChemCatChem, accepted.
[49] M. Armbrüster, M. Behrens, F. Cinquini, K. Föttinger, Yu. Grin, A. Haghofer, B. Klötzer, A. Knop-Gericke, H. Lorenz, A. Ota, S. Penner, J. Prinz, C. Rameshan, Z. Révay, D. Rosenthal, G. Rupprechter, P. Sautet, R. Schlögl, L. Shao, L. Szentmiklósi, D. Teschner, D. Torres, R. Wagner, R. Widmer, G. Wowsnick, ChemCatChem 4 (2012) 1048.
[50] G. Wowsnick, D. Teschner, M. Armbrüster, I. Kasatkin, F. Girgsdies, R. Schlögl, M. Behrens, J. Catal. part II of this work, submitted.
[51] TOPAS version 4.2, copyright 1999, 2009 Bruker AXS.
[52] R. A. Young in: R. A. Young (Ed.) The Rietveld Method, Oxford, Oxford University Press, 1993, p. 1
[53] M. Salmeron, R. Schlögl, Surf. Sci. Rep. 63 (2008) 169.
[54] S. Tanuma, C. J. Powell, D. R. Penn, Surf. Interface Anal. 43 (2011) 689.
[55] Casa XPS Version 2.3.10, 1999.

[56] J. J. Yeh, I. Lindau, Atom. Data Nucl. Data 32 (1985) 1.

[57] J. A. Moulijn, A. E. van Diepen, F. Kapteijn, J. Mol. Catal. A 212 (2001) 3.

[58] H. Kohlmann, J. Solid State. Chem. 183 (2010) 367.

[59] C. Kuhrt, M. Harsdorff, Surf. Sci. 245 (1991) 173.

[60] S. Doniach, M. Sunjic, J. Phys. C 3 (1970) 285.

[61] R. Carli, C. L. Bianchi, Appl. Surf. Sci. 74 (1994) 99.

[62] H. Okamato, J. Phase Equil. 29 (2008) 466.

[63] P. M. T. M. van Attekum, G. K. Wertheim, Phys. Rev. B 43 (1979) 1896.

[64] K. S. Kim, A. F. Gossmann, N. Winograd, Anal. Chem. 46 (1974) 197.

[65] K. Jacobi, Surf. Sci. 192 (1987) 499.